Journal of Membrane Science 493 (2015) 212–223

Contents lists available at ScienceDirect

Journal of Membrane Science

journal homepage: www.elsevier.com/locate/memsci

Novel bilayer well-aligned Nafion/graphene oxide composite membranes prepared using spin coating method for direct liquid fuel cells

Shingjiang Jessie Lue [a,*], Yu-Li Pai [a], Chao-Ming Shih [a], Ming-Chung Wu [a], Sun-Mou Lai [b]

[a] Department of Chemical and Materials Engineering and Green Technology Research Center, Chang Gung University, Kwei-shan, Taoyuan 333, Taiwan
[b] Department of Chemical and Materials Engineering, National Ilan University, I-Lan 260, Taiwan

ARTICLE INFO

Article history:
Received 2 June 2015
Received in revised form
24 June 2015
Accepted 1 July 2015
Available online 4 July 2015

Keywords:
Graphene oxide
Nafion
Composite membrane electrolytes
Spin coating
Fuel cells

ABSTRACT

The objective of this study was to prepare Nafion/graphene oxide (GO) composite membranes for direct liquid fuel cell applications with the aim of decreasing fuel permeability and further increasing cell performance. Nafion 212 (N212) composites of different GO content and local packing density were manufactured using drop coating and spin coating methods. The GO loading in the resulting composites had a positive correlation with the water uptake, ion exchange capacity, and ionic conductivity of the samples. However, the fuel permeability and water diffusivity were not dependent on the GO content in the composite membranes. Rather, the fuel permeability was related to the arrangement, including orientation and local packing density, of the GO in the composites. The Cussler model was used to describe the fuel barrier property of the N212/GO, and the spin-coated composite membranes had a higher effective aspect (width to thickness) ratio, leading to a higher degree of permeability reduction than was achieved in the drop-coated samples. The spin-coated composite with 0.067% GO loading exhibited double peak power densities than the pristine N212 in direct methanol, ethanol, and formic acid fuel cells. The well-aligned thin top layer of GO contributed to the excellent fuel cell performance.

1. Introduction

Direct liquid fuel cells are the devices that convert chemical energy into electrical energy with the feeding of a liquid solution and provide an attractive alternative power source as crude oil prices surge. Among the various feed solutions, formic acid is a strong electrolyte with high kinetic activity [1] and is expected to promote the proton transport in the anode compartment of the fuel cell [2]. Methanol and ethanol have the advantage of high energy density and can be used directly in fuel cells without the need of a hydrogen reforming process [3,4]. Nafion, a perfluorosulfonated polymer, is commonly used as a fuel cell electrolyte material because of its good proton conductivity, mechanical strength, and chemical and thermal stability under fuel cell operating conditions [5,6]. One of the main obstacles that currently limit the performance of direct liquid fuel cells is the fuel cross-over phenomenon through electrolyte membranes. This fuel cross-over leads to a voltage decrease with the increasing current density in the polarization curves [7,8,9]. During fuel cell operation, the liquid fuel solution permeating through the membrane electrolyte from anode to cathode will decrease the cell voltage and efficiency [10,11] and further cause the poisoning of catalysts [12].

Several approaches, such as pore-filling techniques [13,14,15], electron beam grafting [16], and electrospun nanofiber film [17] have recently been proposed to decrease the fuel cross-over phenomenon through electrolyte membranes. Graphene oxide (GO) has attracted attention due to its unique amphiphile [18] and high aspect ratio properties [19]. In addition, GO is a potential filler to block the passage of fuel through the membrane electrolyte. Nair et al. and Paneri et al. proved that a pure GO membrane can significantly block the ethanol and methanol permeation [20, 21] while permitting water vapor diffusion [20]. Lin and Lu demonstrated that the methanol permeability of hot-pressed GO on Nafion membrane was 41% lower than pristine Nafion 115 [17] and such Nafion/GO membrane showed a higher peak power density (55 vs. 38 mW cm^{-2} with a 6 M methanol feed at 50 °C) than Nafion in a direct methanol fuel cell (DMFC). Yuan et al. found suppressed methanol permeability using GO coating onto a Nafion membrane and enhanced DMFC performance (29 vs. 18 mW cm^{-2} with a 2 M methanol feed at 25 °C) [22]. Other studies prepared various Nafion/GO electrolytes from recast GO-containing Nafion solution and confirmed that their methanol permeability was significantly lower than the methanol permeability of pristine

* Corresponding author.
E-mail address: jessie@mail.cgu.edu.tw (S.J. Lue).

http://dx.doi.org/10.1016/j.memsci.2015.07.007
0376-7388/

Nafion film [23– 25]. These works did not attempt to regulate the GO orientation in the recast films.

The barrier property effectiveness of GO compositions can be described using the Cussler model with an aspect ratio of approximately 800 [26]. Lai et al. reported that the apparent aspect ratio can be increased 5 times by crosslinking the GO nanosheet to achieve better barrier function [27]. Further, the GO nanosheets orientation in the polymeric matrix plays an important role in suppressing molecular permeation, as described in the Bharadwaj model [28]: the orientation angle is a dominant parameter in addition to the GO loading and aspect ratio. However, the alignment control of GO nanosheets in composite membranes and its correlation to fuel cell performance have not been studied to the best of our knowledge. In this present study, we fabricated a novel well-aligned N212/GO composite membranes prepared by different coating procedures (drop coating and spin coating) for direct liquid fuel cell applications. The objective was to suppress fuel permeability by varying the loading, packing density, and alignment of GO nanosheets in the composites. The water uptake, water diffusivity, ion exchange capacity, ionic conductivity, and fuel permeability of the composites were evaluated. The performance of the N212/GO composite membranes in a single cell was measured in direct methanol, ethanol, and formic acid fuel cells. The characteristics of the N212/GO composite membranes were also investigated and correlated with the peak power densities of the fuel cells.

2. Experimental

2.1. Materials

Graphite powder ($<20\ \mu m$), isopropanol (99%), and sulfuric acid (95 – 98%) were purchased from Sigma-Aldrich (St. Louis, MO, USA). Potassium permanganate was obtained from Nihon Shiyaku Industries (Osaka, Japan). Nafion dispersion (5 – 6% copolymer resin) and Nafion 212 (N212) membrane were obtained from DuPont Company (Fayetteville, NC, USA). Catalyst Pt black (40% metal particle on carbon, HISPECTM4000) and Pt–Ru black (50% metal particle on carbon, Pt:Ru = 1:1, HISPECTM4000) were obtained from Johnson Matthey (Royston Hertfordshire, UK). Gas diffusion layers (GDLs) with a microporous layer (MPL) (W1S1005, 0.41 mm-thick carbon cloth) and without the MPL (W0S1002, 0.36 mm-thick carbon cloth) were obtained from CeTech Co., Ltd., Taichung, Taiwan. Isopropyl alcohol was purchased from Mallinckrodt Chemicals (St. Louis, MO, USA). Epoxy resin (Epok 812 resin) was obtained from Oken (Tokyo, Japan). Uranyl acetate dihydrate was purchased from Fluka (St. Louis, MO, USA). Pure water with a resistivity of 18 MΩ cm was produced using a Millipore water purifier (Elix 5/Milli-Q Gradient system, Millipore Corp., Bedford, MA, USA).

2.2. Preparation of graphene oxide

Graphene oxide was synthesized from graphite powder using a modified Hummers method [29]. One gram of graphite powder was added to 50 mL concentrated H_2SO_4, and the temperature was controlled below 10 °C using an ice bath. Then, 4 g of $KMnO_4$ was added slowly with stirring. The reaction was continued for 2 h in the ice bath. The mixture was stirred for 1 h and diluted with 50 mL deionized (D.I.) water in the ice bath. The mixture was then further stirred for 1 h and diluted with 50 mL D.I. water. Ten milliliters of 30% H_2O_2 solution was added to the mixture to reduce the remaining $KMnO_4$. The mixture then released a large volume of bubbles and turned to bright yellow. Finally, the mixture was sonicated for 1 h [30]. The product obtained was dialyzed with D.I. water to remove the metal ions. The resulting product was dried in an oven at 60 °C for 24 h.

2.3. Preparation of Nafion 212/GO composite membrane

As a pretreatment, the Nafion 212 membrane was soaked in 5% hydrogen peroxide at 80 °C for 1 h to remove organic matter and was rinsed with D.I. water for 0.5 h. Then, the Nafion was soaked in 1 M sulfuric acid at 80 °C for 1 h to ensure that the membrane had complete converted into an H-type exchange membrane and was rinsed again with D.I. water [14].

2.3.1. Drop coating method

To prepare the different concentrations of GO solutions used in the drop coating method, different amounts (0.02 g and 0.1 g) of GO were dispersed in 10 g of 5 wt% Nafion dispersion (as a binder) with ultrasonication to ensure the uniformity of the mixture. Then, wet N212 membrane was placed in a Petri dish and 2 mL of the above-mentioned GO solutions were dropped onto the top surface. The Nafion/GO composites were dried in a hood to evaporate the solvent and thermally treated at 120 °C for 10 min to avoid having the GO fall off [31]. The actual mass percentages of GO in the composite membranes were determined using gravimetric method. The dry weights of Nafion/GO membranes were by measuring the dry weights before and after the coating procedure. The data were converted weight percentage in the entire composite membrane and the GO weight per unit of area. The GO masses of 0.02 g and 0.1 g resulted in composites with GO contents of 0.28 and 1.49 wt%, respectively, and the resulting membranes were coded with DC-0.28 and DC-1.49, respectively.

2.3.2. Spin coating method

In the spin coating method, an appropriate amount (0.005 g or 0.05 g) of GO was dissolved in 0.10 g of 5 wt% Nafion dispersion, followed by adding 4.95 g of isopropanol and 4.95 g of D.I. water (shown in Table 1) with ultrasonication to form a uniform solution. Wet N212 membrane was placed on a spin coater (model OT-SP101, Olink, New Tapei City, Taiwan), and 2 mL of the above-mentioned dilute Nafion/GO solution were dropped onto the surface. The N212 was spin coated at 500 rpm for 60 s and dried in an oven at 40 °C to remove the excess solvent. The composite membrane was then thermally treated at 120 °C for 10 minutes to avoid having the GO fall off [31]. The actual mass percentages of the GO on the composite membranes were found to be 0.067 and 2.53 wt%, and the composite membranes obtained were coded with SC-0.067 and SC-2.53, respectively.

2.4. Characterization

The microstructure of GO and N212/GO composite membranes

Table 1
GO binder suspension composition and GO loading in prepared N212/GO composite membranes ($n=2$).

Code	GO binder solution composition	GO area loading (10^{-5} g cm^{-2})	GO content (wt%)
N212	–[a]	–[a]	–[a]
DC-0.28	0.02 g GO, 10 g binder solution[b]	4.45	0.28
DC-1.49	0.10 g GO, 10 g binder solution	26.11	1.49
SC-0.067	0.005 g GO, 0.10 g binder solution, 4.95 g IPA[c], 4.95 g water	0.473	0.067
SC-2.53	0.05 g GO, 0.10 g binder solution, 4.95 g IPA, 4.95 g water	14.99	2.53

[a] Not applicable.
[b] Binder solution: 5 wt% Nafion solution.
[c] IPA: isopropyl alcohol.

was observed by using a field emission scanning electron microscope (FESEM) (JSM-7500F, Hitachi High-Technologies Corp., Tokyo, Japan) after sputtering the specimens with Au. The GO sample morphology was obtained with transmission electron microscopy (TEM) (JEM 2000 EXII, JEOL, Tokyo, Japan). The composite membrane sample was dehydrated in a vacuum oven at 60 °C overnight and then embedded in epoxy resin (Epok 812 resin) at 60 °C for 2 days. The specimen was sectioned using an ultramicrotome (Reichert Ultracut S, Leica, Wetzlar, Germany). Ultra-thin sections (approximately 1 μm thickness) were placed on 200 mesh copper grid (Ted Pella Inc., CA, USA) and stained with 0.5% uranyl acetate dihydrate and examined with high resolution transmission electron microscopy (HRTEM) (JEM-2010, JEOL, Tokyo, Japan). Fourier transform infrared (FTIR) spectra of the GO and N212/GO composite membranes were obtained via the attenuated total reflectance (ATR) mode using an FTIR (Perkin–Elmer Spectrum One, Perkin–Elmer Corp., Norwalk, CT, USA) equipped with a multiple internal reflectance apparatus. An X-ray diffraction (XRD, model D5005D, Siemens AG, Munich, Germany) measurement was performed on the GO and N212/GO composite membranes to examine their crystallinity characteristics. The X-ray radiation was generated using Cu Kα (wavelength 1.54 Å) from an anode operating at 40 kV and 40 mA. The scanning rate was $0.5^\circ\ s^{-1}$ with a 0.02° resolution. The XRD was recorded over the angles $10-30^\circ$. The N212/GO composite membranes were analyzed using Raman spectroscopy equipped with a confocal microscope using a 50× objective lens (model inVia, Renishaw, Gloucestershire, United Kingdom) and a charge coupled device detector. The Raman excitation source was provided by a 632.8 nm He–Ne laser beam, which had a beam power of 17 mW with a spot size approximately 1 μm in diameter. The scanning wavelength ranged from 500 to 2000 nm. Densities were measured using a gas pycnometer (AccuPyc II 1340, Micromeritics, Norcross, GA, USA) at room temperature. The diameter and distribution of the suspended GO nanosheets were analyzed using laser scattering analyses (Zetasizer, 2000 HAS, Malvern, Worcestershire, UK) [32]. The aspect ratio of the as-prepared GO was calculated from the GO diameter and thickness.

2.5. Water uptake and diffusivity

The water uptake for pure N212 and N212/GO composite membranes was determined by measuring the difference between the dry weight (W_0, in grams) and the total weight (W_t, in grams) after immersion in D.I. water at room temperature. The water uptake (M, in g g^{-1}) was calculated by the following equation [33, 34]:

$$M = \frac{W_t - W_0}{W_0} \tag{1}$$

where W_0 and W_t are the initial dry and equilibrium membrane weights, respectively.

The water diffusion coefficient was calculated by the limiting slope method [35, 36] using the following equation:

$$\ln\left(1 - \frac{M_t}{M_\infty}\right) = \ln\left(\frac{8}{\pi^2}\right) - \frac{\pi^2 D t}{\delta^2} \tag{2}$$

where M_t and M_∞ denote the water uptake at time t and after the sorption reached a steady state (which represents equilibrium uptake), respectively; D is the diffusion coefficient, and δ is the thickness of the membrane. The slope was obtained from a plot of $\ln(1-M_t/M_\infty)$ vs. time (t) and was equal to $-\pi^2 D/\delta^2$. As a result, the diffusion coefficient could be determined.

2.6. Ion exchange capacity and ionic conductivity measurement

The ion exchange capacity (IEC) of the composite membranes was measured using a titration procedure. Each composite membrane was immersed overnight in 50 mL of 1 M NaCl solution to allow the exchange of protons in the membrane with aqueous sodium ions. The NaCl solution was then titrated with 0.005 M NaOH solution to an end point with phenolphthalein as the indicator. The IEC (Q, in mmol g^{-1}) was calculated from the mass of the dry membrane (W_{dry}), the titrated NaOH volume (V_{base}), and the concentration of the NaOH (C_{base}) [14, 21].

$$Q = \frac{V_{base} \times C_{base}}{W_{dry}} \tag{3}$$

The ionic conductivity of N212/GO composite membranes was measured by sandwiching the membranes between two stainless steel electrodes (with a surface area of 1.33 cm^2 each) in a spring-loaded glass holder, which was maintained under a 99% relative humidity at a preset temperature, ranging from 30 to 80 °C. A potentiostat (Autolab, PGSTAT-30, Eco Chemie B.V., Utrecht, Netherlands) was used to measure the alternative current (AC) impedance of the N212/GO composite membranes. The impedance was scanned from 100 kHz to 100 Hz with an oscillating amplitude of 10 mV. The bulk resistance (R_E, in Ω) of the composite membranes was calculated from the impedance data and derived from the intercept on the real axis of the Nyquist plot [37]. The conductivity (σ, in S cm^{-1}) was calculated using the following equation:

$$\sigma = \frac{L_m}{R_E \times a} \tag{4}$$

where L_m is the thickness of the moistened membranes (cm), and a is the contact area of the stainless steel electrode (1.33 cm^2).

2.7. Formic acid and alcohol permeability measurements

The permeability measurements for formic acid and alcohols, including methanol and ethanol, passing through pure N212 and N212/GO composite membranes were carried out using a handmade, double-jacketed, glass permeation cell as described in our previous paper [38]. The glass cell was divided into two compartments. The donor reservoir compartment was filled with an aqueous solution of fuel (formic acid, methanol, or ethanol), and the receiving reservoir was initially filled with D.I. water. The composite membrane was sandwiched between the two compartments to measure the permeability. The fuel transported through the membranes into the receiving reservoir was determined periodically by using a pH meter (model 6010 pH meter, Jenko Instruments, Inc., San Diego, CA, USA) [39] or a density/specific gravity meter (model DA-130N, Kyoto Electronics Manufacturing Co., Ltd., Kyoto, Japan). The fuel permeability (P, in $cm^2\ s^{-1}$) was calculated using the following equation [40]:

$$P = \frac{slope \times L \times V}{C \times A} \tag{5}$$

where slope represents the plot of the permeated fuel (formic acid, methanol, or ethanol) concentration versus the elapsed time, L is the thickness of the membrane (cm), V is the volume of the receiving reservoir (cm^3), C is the concentration of the solution (mole dm^{-3}), and A is the effective permeation area of the membrane (cm^2).

2.8. Fuel cell test

The catalyst ink was prepared by mixing a predetermined

amount of the catalyst on carbon into a solution of 5 wt% Nafion ionomer solution, D.I. water, and isopropanol under ultrasonication for at least 15 min to obtain a well-dispersed catalyst slurry. The Pt–Ru/C catalyst slurry was then sprayed on the GDL without an MPL for the anode, and the Pt/C catalyst slurry was sprayed on the MPL-containing GDL for the cathode using a spray gun (model GP-2, Fuso Seiki Co., Ltd., Tokyo, Japan) to form gas diffusion electrodes (GDEs) [41]. The cathode GDE contained 5 mg cm^{-2} Pt and the anode GDE contained 5 mg cm^{-2} Pt–Ru. After the GDEs were dried at 40 °C for 2 h, the N212/GO composite membrane was sandwiched between the cathode and anode GDEs to fabricate a membrane electrode assembly (MEA). The active area of the MEA was 1 cm^2. In assembling the single cell, the MEA was enclosed by two Teflon gaskets, each with an opening of 1 cm × 1 cm. Two flow-field plates made of high-density graphite with carved flow paths were fixed next to the MEA and followed by two gold-plated copper end plates as current collectors. Two heating tapes were adhered to the surfaces of the end plates for cell temperature measurement and control. Finally, the single cell assembly was bolted and screwed together using a torque wrench at a torque force of 392 N cm. This experimental apparatus was illustrated in our previous publications [40,42].

The liquid fuel (5 M and 8 M formic acid, 2 M methanol, or 3 M ethanol, which was found to be the optimal fuel concentration [14]) was fed into a thermostatic chamber at 80 °C and recirculated through the anode compartment at a flow rate of 5 mL min^{-1}. Oxygen gas was fed into the cathode at a flow rate of 200 mL min^{-1}. The electrochemical performance (cell voltage and electrical current) of the fuel cell was recorded with a potentiostat (PGSTAT-30, Metrohm Autolab B.V., Utrecht, Netherlands) by measuring the current density at a scan rate of 10 mV s^{-1}, and data were recorded every 50 mV. The power density was calculated as the product of cell voltage and current density. The power density was plotted against the current density (*P–I* curve) to determine the peak power density (P_{max}) at each tested operating condition.

3. Results and discussion

3.1. GO characterizations

The FESEM images in Fig. 1(a) reveal that the prepared GO presented a layered structure with flake-like sheets. When GO was suspended in an aqueous solution the GO exhibited a well dispersed, exfoliated layer structure (Fig. 1(b)). The XRD peak of the pristine graphite was located at 26.7°, corresponding to an inter-planar distance of 0.334 nm. The GO had a strong XRD band at 11.7° (Fig. S1), corresponding to an inter-planar distance of 0.817 nm. The increase in inter-planar distance from 0.335 to 0.817 nm was due to the exfoliation of the graphite sheets, which were oxidized and contained oxygen functional groups at the GO edge [43]. The diameter of the pristine GO was approximately 500 nm using laser scattering analyzer and the GO nanosheets aspect ratio was approximately 500. The GO aspect ratio was similar to the literature values [27].

The FTIR peak at 1626 cm^{-1} was due to C=C stretching. The peak at 1758 cm^{-1} is identified as C=O stretching, and the peak at 1070 cm^{-1} is due to C–O stretching (Fig. S2(a)) [44–46]. Fig. S2 (b) shows the Raman spectra of GO characteristic scattering peaks located at 1329 and 1607 cm^{-1}, corresponding to the D-band and G-band, respectively. The D-band signal represents the sp^3 configuration of the GO carbon bands in the composite membranes. The G-band represents the GO characteristics of the GO. The sp^3 carbon bond configuration caused chemical bond steric orientation and increased the distance between the GO layers. The GO D/G area ratio was higher than that for graphite due to carbon atom oxygenation during the Hummer process.

Fig. 2 shows the full scan, C1s, and O1s spectra of the GO nanoflakes. The GO contained 28 atom% of oxygen, much higher than graphite (1.2 atom%) (Fig. 2(a)). The functional groups were identified by deconvoluting the GO C1s spectra, and the peaks at 284.6, 287.1, and 288.7 eV corresponded to C–C, C–O, and C=O, respectively [47], as shown in Fig. 2(b). O1s spectra curve-fitting revealed the characteristic peaks of C=O (531.4 eV) and C–O (532.9 eV), as shown in Fig. 2(c). The degree of oxidation was approximately 29.0% confirming the formation of oxides [48].

3.2. Morphology of N212/GO composite membranes

This GO was well dispersed in the Nafion binder solution. After the GO-binder solution was applied to the N212 surface via the drop coating or spin coating method, the N212/GO composites were formed. The N212/GO composites were examined for the transmittance values and the results were in the order of N212 > SC-0.067 > SC-2.53 > DC-0.28 > DC-1.49. The photos of the N212/GO composites are also shown in Fig. S3 to reveal the appearance of the various membranes. The spin-coated (SC) samples were more homogeneous than the drop-coated (DC) samples.

The N212/GO composite membranes were also observed using FESEM to examine the surface and side views. As shown in Fig. 3, the surface views indicate GO aggregation in DC-0.28 and DC-1.49 samples. In contrast, the surface structures of SC-0.067 and SC-2.53 were smoother than the surface structures of DC-0.28 and DC-1.49. In addition, the color of the composites implied that the spin coating method could form an evenly distributed coated GO-binder layer on top of the N212 membrane. For the SC composites, SC-2.53 showed some aggregation due to the larger amount of GO loading. The side views of N212/GO composite membranes are shown in Fig. 3, which demonstrates that the recast GO-binder

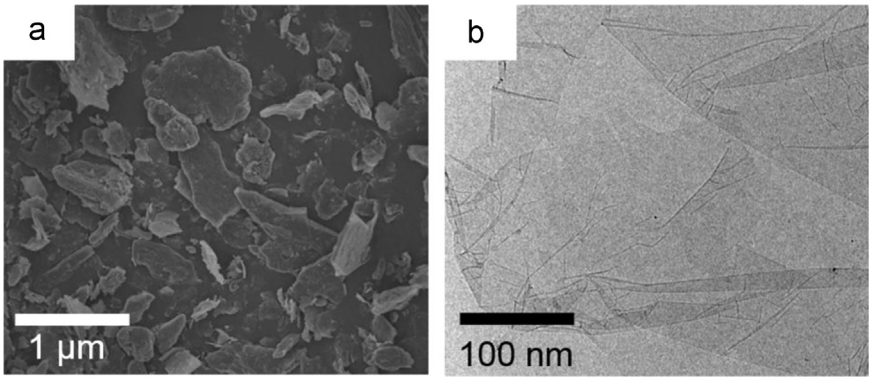

Fig. 1. (a) FESEM images and (b) TEM images of GO.

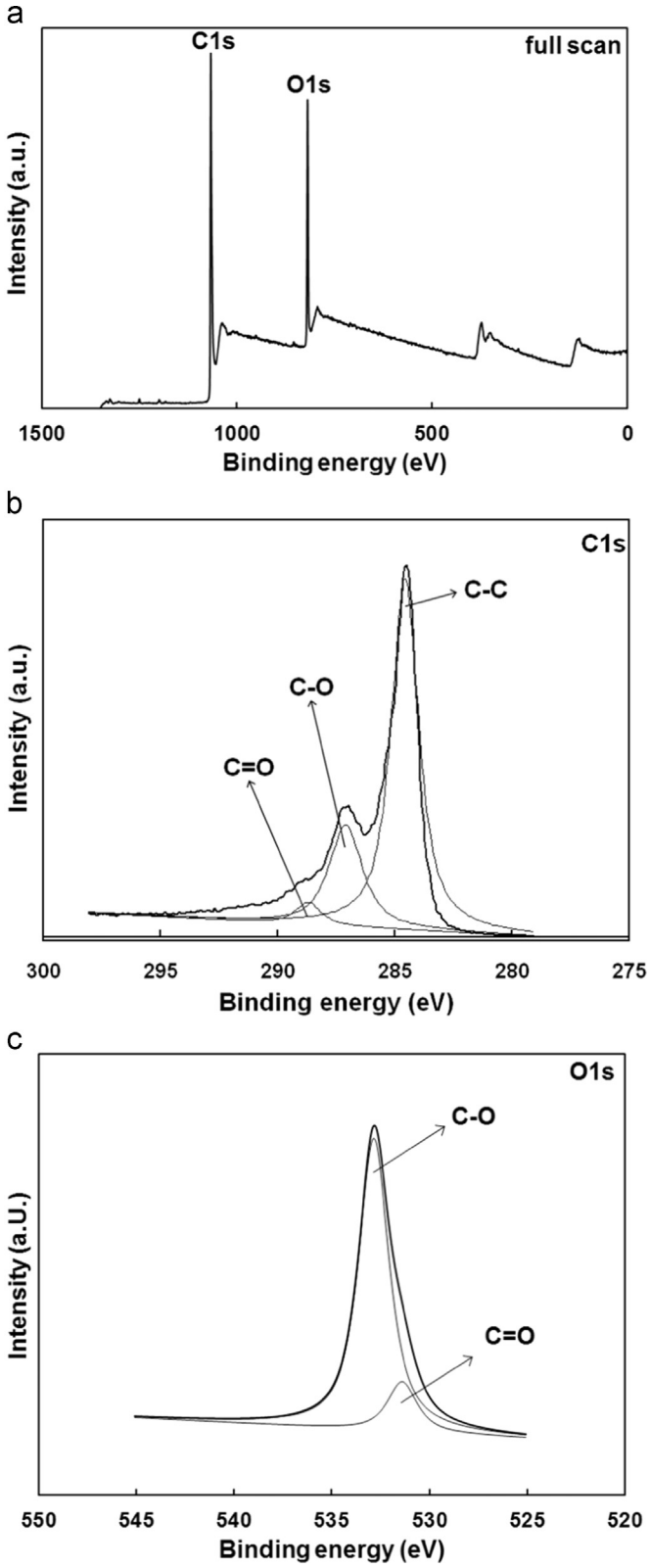

Fig. 2. XPS spectrum and fitting peaks of GO (a) full scan, (b) C1s, and (c) O1s.

layers of DC-0.28 and DC-1.49 were much thicker than the recast GO-binder layers of SC-0.067 and SC-2.53 due to the former's higher binder contents in the GO solutions. The GO loadings based on the area of the DC-0.28 and DC-1.49 were 4.45×10^{-5} and 2.61×10^{-4} g cm^{-2}, respectively (Table 1). The total thicknesses of the Nafion/GO composites were 56 and 60 μm, respectively. The FESEM images indicate that the excess thickness of 11 and 15 μm of the GO-binder was added on top of the N212 for DC-0.28 and DC-1.49, respectively. The GO surface loadings on SC-0.067 and SC-2.53 were 4.73×10^{-6} and 14.99×10^{-5} g cm^{-2} (Table 1), and the additional thicknesses of the GO-binder layers were approximately 1–3 μm, respectively.

3.3. Physicochemical characteristics of N212/GO composite membranes

The crystallinity of N212/GO composite membranes was measured by XRD. The XRD peaks of N212/GO composite membranes were located at 17.6° and 22.6°, mainly ascribed to the N212 component. The XRD peak intensities of N212/GO composite membranes decreased with the increasing GO loading, which implies that the amphiphilic GO sheets were compatible in the two domains of the non-polar backbone and the polar ionic cluster of Nafion [23].

The N212/GO composite membranes are analyzed with ATR-FTIR. The functional groups were located at 1203, 1143, 1054, and 979 cm^{-1}, corresponding to asymmetric and symmetric CF_2 stretching, symmetric SO_3 stretching, and C–O–C stretching, respectively. However, DC-0.28, DC-1.49, and SC-2.53 appeared as three additional peaks compared with SC-0.067 due to the larger amounts of GO loading. Fig. S3 shows the Raman spectra of N212/GO composite membranes. The characteristic scattering peaks were located at 1329 and 1607 cm^{-1}, corresponding to the D-band and G-band, respectively. The peak intensities increased with the increasing GO loading. From the above instrumental analysis, the composites were confirmed to exhibit the characteristics from the GO and the N212.

3.4. Ion exchange capacity, water uptake, and ionic conductivity

The data of IEC, water uptake, and ionic conductivity for the N212/GO composite membranes and the pristine N212 are shown in Table 2. At room temperature, the IEC and water uptake of the pristine N212 were 0.87 mmol g^{-1} and 0.277 g g^{-1}, respectively, in agreement with data from the literature [17]. The IEC and water uptake values decreased with the increasing GO loading. The IEC values for SC-0.067, DC-0.28, DC-1.49, and SC-2.53 were 0.82, 0.79, 0.76, and 0.55 mmol g^{-1}, respectively. The water uptakes of SC-0.067, DC-0.28, DC-1.49, and SC-2.53 were 0.271, 0.266, 0.203, and 0.129 g g^{-1}, respectively. The incorporation of GO into the N212 membrane caused the decrease of IEC and water uptake due to the hydrophobic nature of the sp^2 domain (i.e., C=C bonds) in the GO. Moreover, the compatibility of the amphiphilic GO sheets with the polar ionic cluster of Nafion might result in steric hindrance and obstruct the sorption of water molecules in the ionic cluster of the Nafion matrix.

The water uptake of N212 of 0.277 g g^{-1} corresponded to 17 water molecules per sulfonate group (Fig. S5). The samples with the low GO content (DC-0.28 and SC-0.067) showed similar water sorption capacities. The high GO content composites (DC-1.49 and SC-2.53) sorbed a smaller amount of water than estimated by taking IEC into consideration. The measured data were 12.4 and 7.8 water molecules per sulfonate group for DC-1.49 and SC-2.53, respectively. Assuming that each sulfonate group in DC-1.49 and SC-2.53 would adsorb the same (17) water molecules as the N212, the estimated values based on the measured IEC would be 14.8 and 10.7 water molecules per sulfonate group (as shown by the straight line in Fig. S5). The further reduction in water uptake in the high GO samples may be caused by the steric confinement of the GO nanosheets. The steric confinement restricts the cluster size expansion upon solvation.

The resistance and ionic conductivity data of the pristine N212

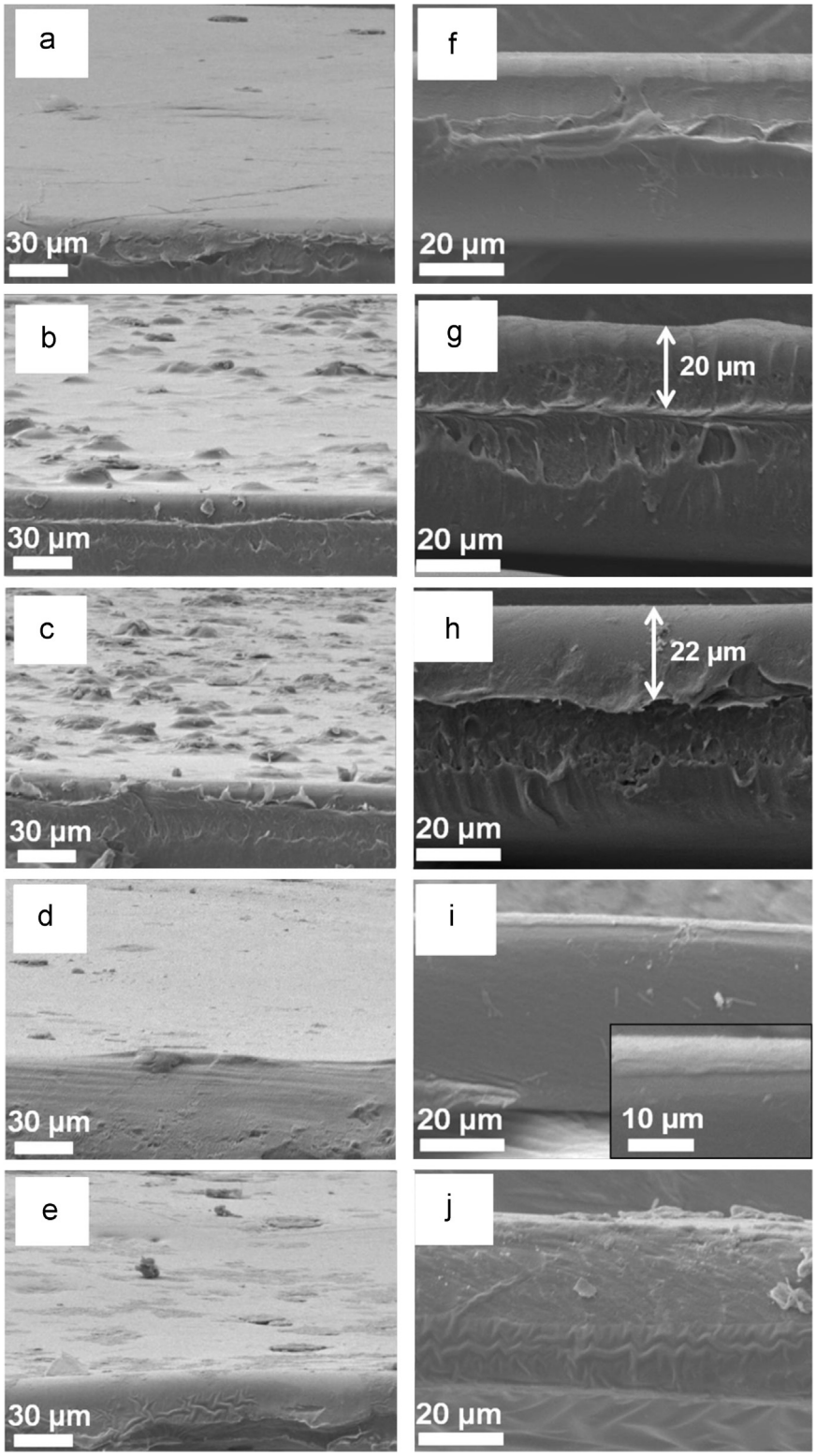

Fig. 3. Surface views of N212/GO composite membranes (a) N212; (b) DC-0.28; (c) DC-1.49; (d) SC-0.067; (e) SC-2.53 and their cross-sectional views (f) N212; (g) DC-0.28; (h) DC-1.49; (i) SC-0.067; (j) SC-2.53.

and N212/GO composite membranes were measured using the AC impedance analyzer. The pristine N212 had the highest ionic conductivity, 11.76×10^{-3} S cm^{-1}, compared with the other N212/GO composite membranes at 80 °C. The addition of GO decreased the water uptake and IEC of N212/GO composite membranes due to the hydrophobic sp^2 domain, as described above. The lower water uptake and IEC inhibited the transport of ions in the ionic sulfonate clusters of N212/GO composite membranes. As a result, the ionic conductivity of N212/GO composite membranes decreased with the increasing GO loading. The ionic conductivities of SC-0.067, DC-0.28, DC-1.49, and SC-2.53 were 10.56, 9.90, 9.41, and 5.92×10^{-3} S cm^{-1}, respectively (Table 2). Although Kumar et al. showed that the blended GO (4%) composite membrane had higher conductivity than recast Nafion and Nafion 212 [49]. Lin

Table 2
Ion exchange capacity, water uptake, and ionic conductivity in N212/GO composite membranes.

	Ion exchange capacity[a] (mmol g^{-1})	Water uptake[a] ($g\,g^{-1}$)	Ionic conductivity[b] (10^{-3} S cm^{-1})
N212	0.87	0.277	11.76
SC-0.067	0.82	0.271	10.56
DC-0.28	0.79	0.266	9.90
DC-1.49	0.76	0.203	9.41
SC-2.53	0.55	0.129	5.92

[a] At room temperature.
[b] At 80 °C.

and Lu and Choi et al. reported that the conductivity of the Nafion/GO membrane was lower than Nafion 115 [17, 23]. Our drop-coated and spin-coated samples demonstrated conductivity decreases in the GO composites, in agreement with the later reports.

3.5. Permeability and water diffusivity

Table S1 shows the permeability at different concentrations of formic acid, methanol and ethanol solutions for the N212 membrane and N212/GO composite membranes at 80 °C. For 5 M and 8 M formic acid solutions, the permeability value of the pristine N212 was the highest among the tested membranes, followed by DC-0.28, DC-1.49, SC-0.067, and SC-2.53. The formic acid permeability values of the spin-coated samples were the lowest among the composites, most likely because the spin-coated samples exhibited a flat and smooth surface with an even coverage of the GO sheets. The well-aligned GO barrier layer generated more tortuous diffusion paths and prohibited the formic acid permeation. The GO binder suspension used for the spin-coating had a lower binder content and result in a thinner top layer. The spinning force and the low binder content resulted in an orientation where the GO nanosheets were tightly stacked with less distance between the nanosheets, which effectively slowed down fuel permeation. As a result, the arrangement of GO on the membrane surface, rather than the GO content, was the main factor that affected the permeability of the N212/GO composite membranes.

For the 2 M methanol and 3 M ethanol solutions, the permeability values were one order of magnitude lower than the permeability values from the formic acid solutions (Table S1). The GO-containing samples suppressed alcohol permeation when compared with the N212. Again, the alcohol permeability of SC-0.067 was the lowest, only 32–60% of that of the pristine N212 for the same reasons as described above. Lin and Lu [17] reported that the methanol permeability of the hot-pressed GO on Nafion 115 membrane decreased 41% with the 1 M methanol solution at 35 °C. Yuan et al. [22] found the methanol permeability of GO coating on Nafion membrane was 73% lower than pristine Nafion. Choi et al. [23, 24] observed a 39% reduction in methanol permeability in the composite of 0.5 wt% GO in a recast Nafion membrane. GO has been demonstrated to be an effective methanol barrier but we demonstrated herein that the degree of permeability decrease was not solely governed by the GO content.

The water diffusivity measurement was performed on the composites using a gravimetric method, and the data are included in Fig. S6. The data show a linear relationship between the water diffusivity and the formic acid permeability with the 5 M solution. Both water diffusivity and fuel permeability are slightly dependent on the GO content. The GO content seems likely to affect the water sorption behavior and the IEC (Table 2) but hardly explains the diffusion behavior; more factors need to be investigated to elucidate the complicated fuel transport phenomena.

3.6. Fuel cell performance

3.6.1. Direct formic acid fuel cell performance

The direct formic acid fuel cell performance of the SC-0.067 and SC-2.53 composite membranes was measured and compared at a 1 M concentration of fuel at 80 °C. As shown in Fig. S7(a), the open circuit voltage (OCV) of SC-2.53 (0.44 V) was much lower than SC-0.067 (0.65 V). The SC-2.53 (Fig. 3(e)) had a rougher surface than SC-0.067 (Fig. 3(d)) and created interfacial electrical resistance in the single cell. The lower formic acid permeability of the SC-2.53 should have been beneficial for the cell voltage [9], but the much lower ionic conductivity of SC-2.53 (Table 2) caused a severe ohmic overpotential [9]. The cell voltage was therefore lower in the fuel cell with the SC-2.53 electrolyte over the entire current density range (Fig. S7(a)).The lower water uptake in SC-2.53 also impeded the transport of hydrated H^+ ions, leading to a lower local proton concentration at the cathode and producing a lower electrical current. Moreover, FESEM showed that the surface of SC-2.53 demonstrated aggregation of GO, and the uneven surface may cause interfacial resistance and retard the mass transport rate of the reactants. The peak power density of SC-2.53 was 60.1% lower than the peak power density of SC-0.067 (21.8 vs. 54.7 mW cm^{-2}) (Fig. S7(b)). The current densities corresponding to the peak power densities of SC-2.53 and SC-0.067 were 66.4 and 145 mA cm^{-2}, respectively. In conclusion, the SC-0.067 outperformed SC-2.53, and the SC-0.067 was further tested and compared with other membrane electrolytes.

When SC-0.067 was compared with the N212 membrane for fuel cells fed with 5 M and 8 M formic acid, the SC-0.067 membrane demonstrated performance superior to the N212. As shown in Fig. 4(a) and (b), the OCV of the pristine N212 was much lower than the OCV of SC-0.067 (0.48 vs. 0.67 V, Fig. 4(a)) due to the higher permeability (Table S1), which makes the fuel cell prone to fuel cross-over. The peak power density of composite SC-0.067 was 127% higher than the peak power density of pristine N212 (163 vs. 71.5 mW cm^{-2}) with 5 M formic acid at 80 °C (Fig. 4(b)). As the concentration of formic acid increased from 5 to 8 M, the peak power density of SC-0.067 decreased from 163 to 133 mW cm^{-2} due to the higher formic acid cross-over rate, which resulted from a slightly higher permeability (1.31×10^{-5} vs. 1.4×10^{-5} $cm^2\,s^{-1}$) and double fuel concentration. The peak power density of N212 declined from 71.5 to 45.7 mW cm^{-2} with the same formic acid concentration increase. The addition of a very small amount of GO could significantly decrease the permeability and improve the fuel cell performance. These peak power density results corresponded to the ratios of the selectivity, in terms of ionic conductivity versus fuel permeability, shown in Table S2. However, the concentrated formic acid fuel could sustain a higher current density, up to 1100 mA cm^{-2} and generated a higher peak power density at a region higher than 800 mA cm^{-2}.

3.6.2. Direct alcohol fuel cell performance

The cell performance of the pristine N212 and N212/GO composite membranes with 2 M methanol at 80 °C is shown in Fig. 5 (a) and (b). The peak power densities of pristine N212, DC-0.28, DC-1.49, and SC-0.067 were 55, 63, 66, and 113 mW cm^{-2}, respectively (Fig. 5(b)). The SC-0.067 composite had the highest peak power density due to having the lowest permeability and higher conductivity/permeability selectivity (Table S2). Furthermore, the rougher surface of the drop-coated samples (DC-0.28 and DC-1.49, Fig. 3) might cause the larger interfacial resistance between the electrolyte membrane and the GDEs, decreasing the fuel cell voltage. The SC-0.067 sample exhibited a 105% increase in the P_{max}, significantly higher than non-orientated GO composites (18–57% increase in P_{max}[23, 24, 25]).

However, as 3 M ethanol was fed to the fuel cell, the peak

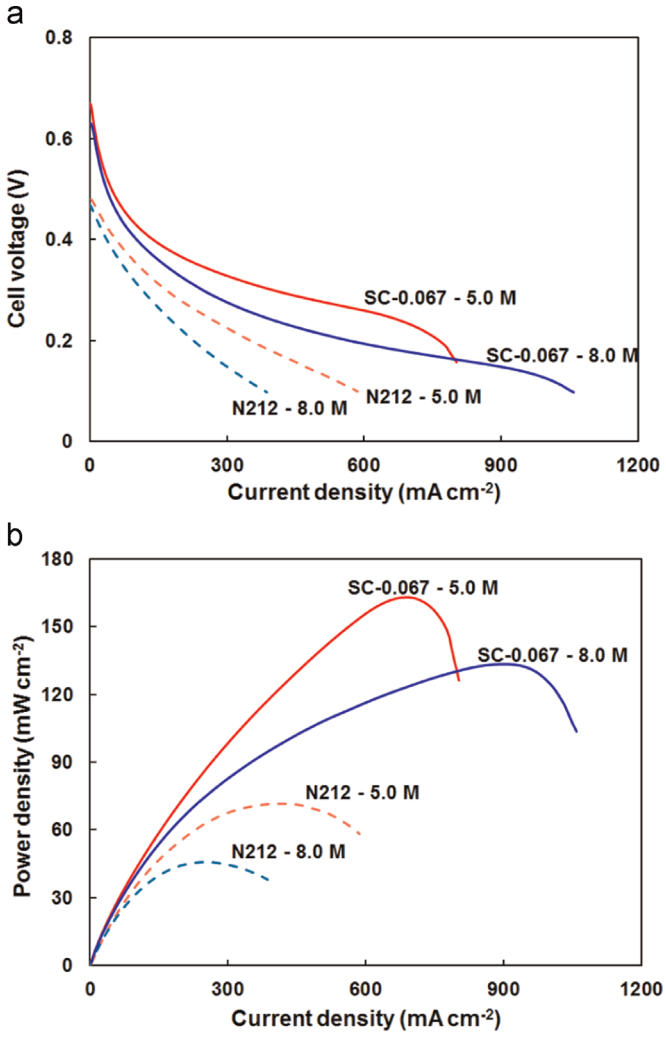

Fig. 4. Direct formic acid fuel cell performance: (a) *V–I* curve (b) *P–I* for N212 and SC-0.067 composite membrane fed with 5 M and 8 M formic acid at 80 °C (anode: formic acid at a flow rate of 5 mL min^{-1}, cathode: oxygen at a flow rate of 200 mL min^{-1}).

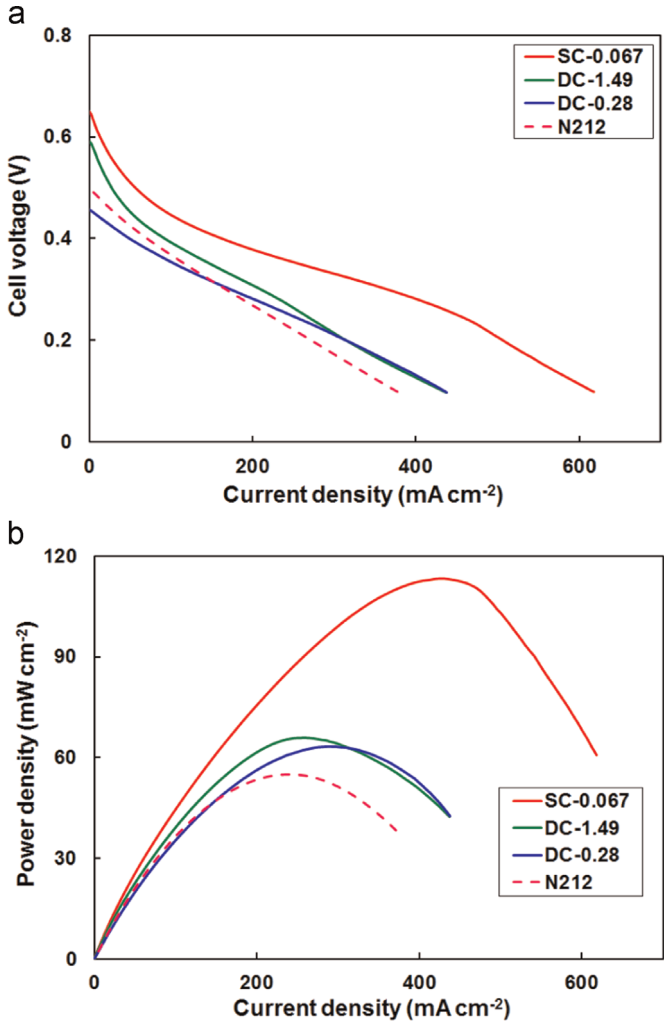

Fig. 5. Direct methanol fuel cell performance: (a) *V–I* curve (b) *P–I* curve for N212 and N212/GO composite membranes at 80 °C (anode: 2 M methanol with a flow rate of 5 mL min^{-1}, cathode: oxygen with a flow rate of 200 mL min^{-1}).

power densities of all composite electrolytes decreased significantly (Fig. 6(a) and (b)) due to the lower catalyst activity efficiency: breaking C–C bonds in the ethanol molecules is usually not complete, and other oxidation by-products are formed, reducing the Gibb's free energy with lower cell voltage [9]. Nevertheless, SC-0.067 generated more than double peak power density compared with N212 (Fig. 5(b)).

3.7. Arrangement of GO on composite membranes

From the above results, we observed that many characterizations pertinent to direct liquid fuel cell performance were not necessarily correlated with GO loading level but with the arrangement of GO in the composite membranes. Dreyera et al. showed that hydrogen bonding occurs between GO and water molecules [50]. This would increase the apparent GO aspect ratio. If GO nanosheets form parallel well-aligned layers, the increased aspect ratio would further affect permeant transport property [27]. To illustrate this effect, the Cussler model [19,51] and Bharadwaj model [28] were used to investigate the barrier property of the composites as a result of the effective aspect ratio of GO. The Cussler model is useful to predict the permeation reduction in a composite membrane due to parallel sheet filler incorporation:

$$\frac{P_0}{P_c} = 1 + \alpha^2 \frac{\varphi^2}{1-\varphi} \tag{6}$$

where P_0 and P_c represent the fuel permeability of the pristine membrane and composite membrane, respectively. The parameter α is the aspect ratio, and ϕ is the volume fraction of GO (calculated from the GO weight percentage and of GO and Nafion densities) (the true density is 1.94 g cm^{-3} for GO and 1.82 g cm^{-3} for N212). The Cussler model is applicable when the filler concentration is at the semidilute condition, assuming that $\phi \ll 1.0$ and $\alpha\phi > 1.0$. In this study, the reference P_0 value is taken as the same as the N212 membrane for SC samples, as the top layer was only 1–2 μm. The Bharadwaj model is useful to predict the permeation reduction in a composite membrane due to non-oriented random array sheet filler incorporation:

$$\frac{P_0}{P_c} = \frac{1-\varphi}{[1 + \frac{\alpha\varphi(2(\frac{(3\cos^2\theta - 1)}{2}) + 1)}{6}]} \tag{7}$$

where θ is the angle between the direction and the normal of the layer alignment. However, the reference P_0 value is for a specimen with a recast thin Nafion binder layer of 20 μm thickness on top of N212 for DC samples to take the thickness increase into consideration and to reflect the GO effect on permeability.

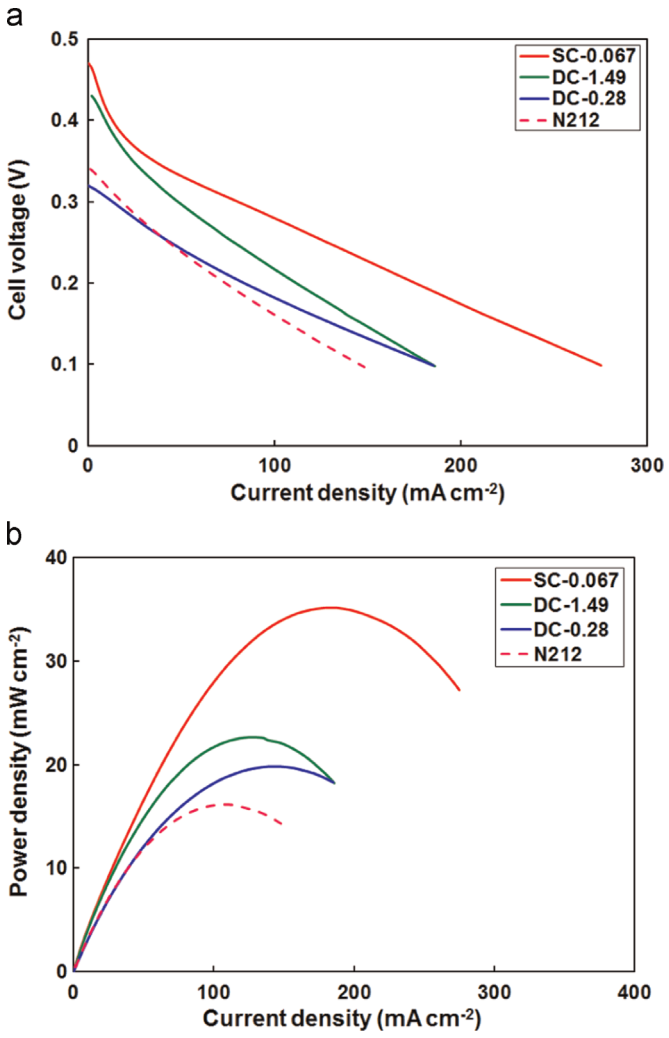

Fig. 6. Comparison of direct ethanol fuel cell performance: (a) *V–I* curve (b) *P–I* curve of N212 and N212/GO composite membranes at 80 °C (anode: 3 M ethanol with a flow rate of 5 mL min^{-1}, cathode: oxygen with a flow rate of 200 mL min^{-1}).

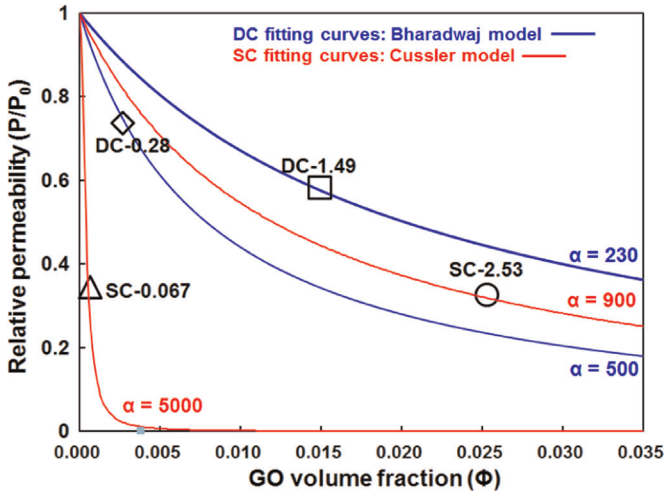

Fig. 7. Relationship of relative permeability for 5 M formic acid through N212/GO composite membranes as a function of volume fraction of GO at various aspect ratios (α). The lines are plotted using the Cussler and Bharadwaj models.

Fig. 7 shows the relationship of relative permeability from 5 M formic acid as a function of the GO volume fraction for the tested N212/GO composites. The GO on the DC samples did not have a particular arrangement and the Bharadwaj model (Eq. (7), assumed θ=60°) was used to describe the permeability behavior. The fitted α value for DC-0.28 was 500, which was close to the pristine GO aspect ratio. This indicates that the dilute GO was randomly arranged in the binder polymer. The α value of DC-1.49 decreased to 230, which was due to the aggregation and stacking in forming thicker pellets [28]. The SC samples exhibited flat and aligned GO orientation on the surface and the Cussler model (Eq. (6)) was employed to determine the GO barrier property. The fitted α values were 900 and 5000 for SC-2.53 and SC-0.067, respectively. The more concentrated GO suspension used for SC-2.53 (Table 1) may have caused GO aggregate stacking and reduced

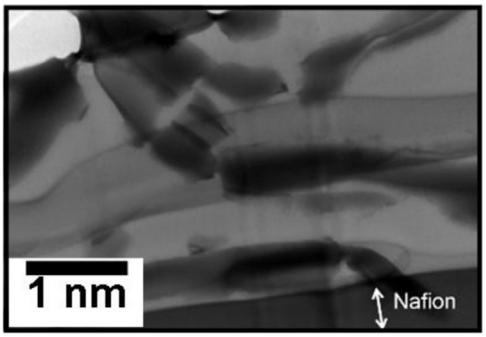

Fig. 8. High resolution TEM cross-section image of SC-2.53 composite membranes.

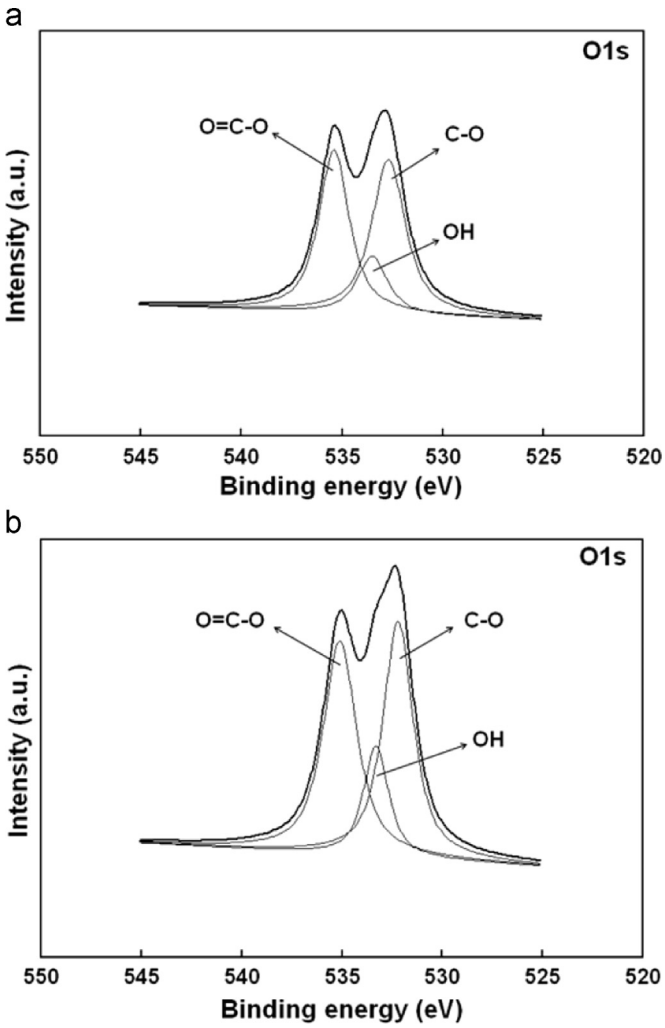

Fig. 9. XPS O1s spectra and fitting peaks of (a) DC-0.28 and (b) SC-0.067.

apparent aspect ratio.

In order to demonstrate the GO alignment levels, HRTEM and XPS analysis were performed on the composites. Fig. 8 reveals the SC-2.53 composite cross-section. The GO layers formed parallel alignment on the surface. The XPS O1s spectra peaks were DC-1.49 and SC-0.067 as shown in Fig. 9(a) and (b). The deconvoluted O1s peaks were associated with C–O, O=C–O, and OH groups [48,52]. The hydroxyl groups are associated with the hydrogen bond between the GO nanosheets [50]. The hydroxyl peak area divided by the overall peak area of SC-0.067 (16.3%) was higher than of DC-0.28 (14.6%), implying that more hydrogen bonds existed in the SC-0.067 sample. The increased apparent aspect ratio of the GO nanosheets in the SC-0.067 composite is proposed and illustrated in Fig. 10.

The less aligned GO created less tortuous transport paths for the permeants (Fig. 11) and led to a slight decrease of permeability. In contrast, the larger aspect ratio of composite SC-0.067 caused a substantial decrease of permeability. The well-aligned GO barrier layer generated tortuous diffusion paths and prohibited the formic acid permeation. In addition, the spinning force and the low binder content resulted in an orientation where the GO nanosheets form parallel tight stacks, leading to increases in the effective aspect ratio of the GO sheets. The fuel encountered higher resistance to its permeation through this binder region with the quasi-connected GO nanosheets (Fig. 11). In conclusion, both the GO content and the alignment in the N212/GO composite membranes play key roles in permeability suppression.

4. Conclusion

The N212/GO composite membranes were prepared by drop coating and spin coating methods to prepare electrolytes for direct liquid fuel cell applications. The GO was used as a barrier to suppress fuel cross-over in the N212/GO composite membranes. The GO loading affects the sorption-related behaviors, including IEC, water uptake, and ionic conductivity. However, diffusion and permeability properties are related to both GO level and the alignment of the GO nanosheets. The Cussler model was used to elucidate the arrangement and alignment of the GO in the composite membranes. The spin-coated composite membrane SC-0.067 had a thin top GO layer of 1–2 μm, with low GO content (0.067 wt% and 4.73×10^{-6} g cm^{-2}) but extremely even coverage on the N212 surface. This sample demonstrated parallel orientation to the surface with a high local packing density, which resulted in the highest effective aspect ratio among the membranes. SC-0.067 also exhibited the lowest formic acid, methanol, and ethanol permeability compared with pristine N212 and other composite membranes. The peak power densities of SC-0.067 with formic acid, methanol, and ethanol fuels at 80 °C were 163, 113, and 35 mW cm^{-2}, respectively. These data doubled the performance of the pristine N212 membrane. The composite membrane SC-0.067 contained well-aligned GO and achieved the highest cell performance with a small amount of GO content. In conclusion, the characteristics of the N212/GO composite membranes were attributed not only to the GO loading but also to the arrangement of GO sheets on the composite surface. The spin coating method is an easy and effective way to prepare polymer/GO composites and exhibited a potential for direct liquid fuel cell applications.

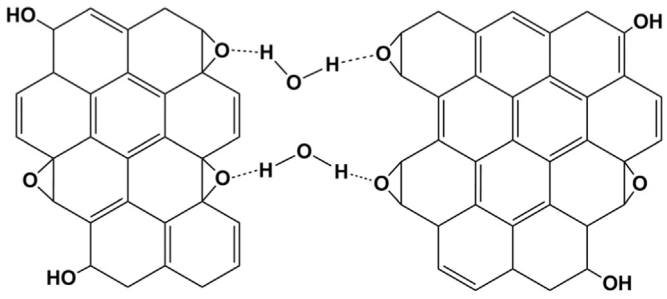

Fig. 10. Supposed hydrogen bonding formed between oxygen functionality on water and GO.

Acknowledgments

The authors wish to acknowledge the financial support of the Ministry of Science and Technology, Taiwan (MOST 103-2221-E-182-064-MY3) and Chang Gung Memorial Hospital, Taiwan (CMRPD2D0151).

Appendix A. Supplementary Information

Supplementary data associated with this article can be found in the online version at http://dx.doi.org/10.1016/j.memsci.2015.07.007.

Nomenclature

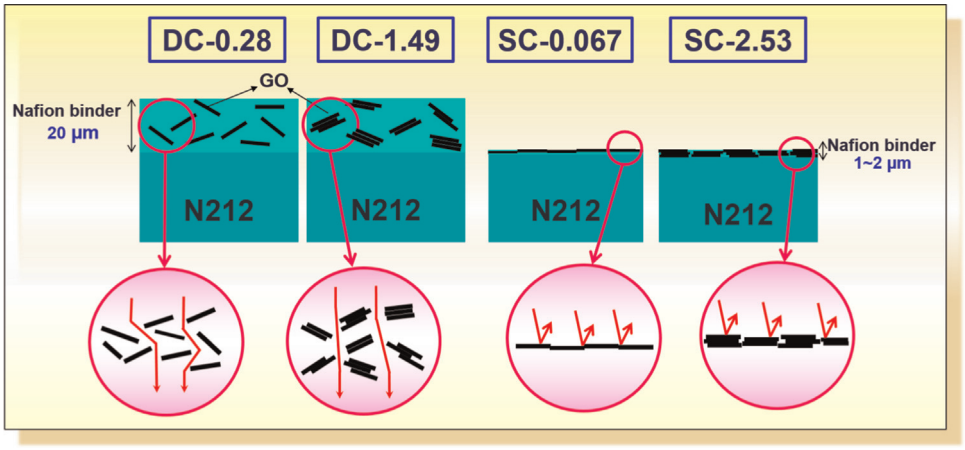

Fig. 11. Schematic diagram of fuel permeation in N212/GO composite membranes.

A	Effective permeation area of the membrane (cm^2)
a	Working area of stainless electrode (cm^2)
C	Initial fuel concentration (mole dm^{-3})
Cbase	NaOH concentration (mole dm^{-3})
D	Water diffusion coefficient ($cm^2\ s^{-1}$)
L	Thickness of the membrane (cm)
L_m	Thickness of moistened membrane (cm)
M	Water uptake of membrane (dimensionless)
M_t	Water uptake in membrane at time t (g)
M_∞	Water uptake in membrane at equilibrium (g)
P	Fuel permeability coefficient ($cm^2\ s^{-1}$)
P_0	Fuel permeability of the pristine membrane ($cm^2\ s^{-1}$)
P_c	Fuel permeability of the composite membrane ($cm^2\ s^{-1}$)
Q	Ion exchange capacity (mmol g^{-1})
R_E	Electrolyte resistance (Ω)
V	Volume of receiving reservoir (cm^3)
V_{base}	Volume of titrated NaOH (cm^3)
W_0	Initial weight of dry membrane (g)
W_{dry}	Mass of dry membrane (g)
W_t	Weight of membrane at time intervals (g)
α	Aspect ratio (dimensionless)
θ	Angle between the direction of the normal of the layers (degree)
ϕ	GO volume fraction (dimensionless)
δ	Membrane thickness (cm)
σ	Conductivity of membrane electrolyte (S cm^{-1})

References

[1] S. Ha, Z. Dunbar, R.I. Masel, Characterization of a high performing passive direct formic acid fuel cell, J. Power Sources 158 (2006) 129–136.
[2] C. Rice, S. Ha, R.I. Masel, P. Waszczuk, A. Wieckowski, T. Barnard, Direct formic acid fuel cells, J. Power Sources 111 (2002) 83–89.
[3] M. Waidhas, W. Drenckhahn, W. Preidel, H. Landes, Direct-fuelled fuel cells, J. Power Sources 61 (1996) 91–97.
[4] J. Ge, H. Liu, Experimental studies of a direct methanol fuel cell, J. Power Sources 142 (2005) 56–69.
[5] S.R. Samms, S. Wasmus, R.F. Savine, Thermal stability of Nafion® in simulated fuel cell environments, J. Electrochem. Soc. 143 (1996) 1498–1504.
[6] T. Okada, S. Moller-Holst, O. Gorseth, S. Kjelstrup, Transport and equilibrium properties of Nafion membranes with H^+ and Na^+ ion, J. Electrochem. Soc. 442 (1998) 137–145.
[7] K. Scott, W. Taama, J. Cruickshank, Performance and modeling of a direct methanol solid polymer electrolyte fuel cell, J. Power Sources 65 (1997) 159–171.
[8] G. Murgia, L. Pisani, A.K. Shukla, K. Scott, A numerical model of a liquid–feed solid polymer electrolyte DMFC and its experimental validation, J. Electrochem. Soc. 150 (2003) A1231–A1245.
[9] B.Y. Wang, H.K. Lin, N.Y. Liu, K.P.O. Mahesh, S.J. Lue, Cell performance modeling of direct methanol fuel cells using proton-exchange solid electrolytes: effective reactant diffusion coefficients in porous diffusion layers, J. Power Sources 227 (2013) 275–283.
[10] W.H. Pan, S.J. Lue, C.M. Chang, Y.L. Liu, Alkali doped polyvinyl alcohol/multi walled carbon nano-tube electrolyte for direct methanol alkaline fuel cell, J. Membr. Sci. 376 (2011) 225–232.
[11] C.F. Lo, J.F. Wu, H.Y. Li, W.S. Hung, C.M. Shih, C.C. Hu, Y.L. Liu, S.J. Lue, Novel polyvinyl alcohol nanocomposites containing carbon nano-tubes with Fe_3O_4 pendants for alkaline fuel cell applications, J. Membr. Sci. 444 (2013) 41–49.
[12] T.C. Deivaraj, J.Y. Lee, Preparation of carbon-supported PtRu nanoparticles for direct methanol fuel cell applications-a comparative study, J. Power Sources 142 (2005) 43–49.
[13] A. Kuzume, Y. Miki, M. Ito, Characterisation of PAMPS–PSS pore-filling membrane for direct methanol fuel cell, J. Membr. Sci. 446 (2013) 92–98.
[14] B.Y. Wang, C.K. Tseng, C.M. Shih, Y.L. Pai, H.P. Kuo, S.J. Lue, Polytetrafluoroethylene (PTFE)/silane cross-linked sulfonated poly(styrene–ethylene/butylene–styrene) (sSEBS) composite membrane for direct alcohol and formic acid fuel cells, J. Membr. Sci. 464 (2014) 43–54.
[15] T.H. Nguyen, C. Wang, X. Wang, Pore-filling membrane for direct methanol fuel cells based on sulfonated poly(styrene-ran-ethylene) and porous polyimide matrix, J. Membr. Sci. 342 (2009) 208–214.
[16] R. Tsuchida, S. Hiraiwa, A. Tsukamoto, M. Washio, A. Oshima, Fabrication of function-graded proton exchange membranes for direct methanol fuel cells using electron beam-grafting, Fuel Cells (2014) 284–290.
[17] C.W. Lin, Y.S. Lu, Highly ordered graphene oxide paper laminated with a Nafion membrane for direct methanol fuel cells, J. Power Sources 237 (2013) 187–194.
[18] L.J. Cote, F. Kim, J. Huang, Langmuir-blodgett assembly of graphite oxide single layers, J. Am. Chem. Soc. 131 (2009) 1043–1049.
[19] E.L. Cussler, S.E. Hughes, W.J. Ward III, R. Aris, Barrier membranes, J. Membr. Sci. 38 (1988) 161–174.
[20] R.R. Nair, H.A. Wu, P.N. Jayaram, I.V. Grigorieva, A.K. Geim, Unimpeded permeation of water through helium-leak-tight graphene-based membranes, Science 335 (2012) 442–444.
[21] A. Paneri, Y. He, G. Ehlert, A. Cottrill, H. Sodano, P. Pintauro, S. Moghaddam, Proton selective ionic graphene-based membrane for high concentration direct methanol fuel cells, J. Membr. Sci. 467 (2014) 217–225.
[22] T. Yuan, L. Pu, Q. Huang, H. Zhang, X. Li, H. Yang, An effective methanol-blocking membrane modified with grapheneoxide nanosheets for passive direct methanol fuel cells, Electrochim. Acta 117 (2014) 393–397.
[23] B.G. Choi, Y.S. Huh, Y.C. Park, D.H. Jung, W.H. Hong, H. Park, Enhanced transport properties in polymer electrolyte composite membranes with graphene oxide sheets, Carbon 50 (2012) 5395–5402.
[24] B.G. Choi, J. Hong, Y.C. Park, D.H. Jung, W.H. Hong, P.T. Hammond, H. Park, Innovative polymer nanocomposite electrolytes: nanoscale manipulation of ion channels by functionalized graphenes, ACS Nano 5 (2011) 5167–5174.
[25] H.C. Chien, L.D. Tsai, C.P. Huang, C. Kang, J.N. Lin, F.C. Chang, Sulfonated graphene oxide/Nafion composite membranes for high-performance direct methanol fuel cells, Int. J. Hydrog. Energy 38 (2013) 13792–13801.
[26] H.D. Huang, C.Y. Liu, D. Li, Y.H. Chen, G.J. Zhong, Z.M. Li, Ultra-low gas permeability and efficient reinforcement of cellulose nanocomposite films by well-aligned graphene oxide nanosheets, J. Mater. Chem. A 2 (2014) 15853–15863.
[27] C.L. Lai, J.T. Chen, Y.J. Fu, W.R. Liu, Y.R. Zhong, S.H. Huang, W.,S. Hung, S.J. Lue, C. C. Hu, K.R. Lee, Bio-inspired cross-linking with borate for enhancing gas-barrier properties of poly(vinyl alcohol)/graphene oxide composite films, Carbon 82 (2015) 513–522.
[28] R.K. Bharadwaj, Modeling the barrier properties of polymer-layered silicate nanocomposites, Macromolecules 34 (2001) 9189–9192.
[29] X. Shen, L. Jiang, Z. Ji, J. Wu, H. Zhou, G. Zhu, Stable aqueous dispersions of graphene prepared with hexamethylenetetramine as a reductant, J. Colloid Interf. Sci. 354 (2011) 493–497.
[30] L.D. Tsai, H.C. Chien, W.H. Huang, C.P. Huang, C.Y. Kang, J.N. Lin, F.C. Chang, Novel bilayer composite membrane for passive direct methanol fuel cells with pure methanol, Int. J. Electrochem. Sci. 8 (2013) 9704–9713.
[31] Z. Siroma, N. Fujiwara, T. Ioroi, S. Yamazaki, K. Yasuda, Y. Miyazaki, Dissolution of Nafion® membrane and recast Nafion® film in mixtures of methanol and water, J. Power Sources 126 (2004) 41–45.
[32] S.J. Lue, Y.L. Wu, Y.L. Tung, C.M. Shih, Y.C. Wang, J.R. Li, Functional titanium oxide nano-particles as electron lifetime, electrical conductance enhancer, and long-term performance booster in quasi-solid-state electrolyte for dye-sensitized solar cells, J. Power Sources 274 (2015) 1283–1291.
[33] S.J. Lue, S.J. Shieh, Modeling water states in polyvinyl alcohol-fumed silica nano-composites, Polymer 50 (2009) 654–661.
[34] S.J. Lue, S.W. Yang, Sorption of organic solvents in poly(dimethyl Siloxane) membrane. I. Permeant states quantification using differential scanning calorimetry, J. Macromol. Sci. Phys. 44 (2005) 711–725.
[35] S.J. Lue, T.H. Yang, K.S. Chang, K.L. Tung, Water diffusivity suppression and ethanol-over-water diffusion selectivity enhancement for ethanol/water mixtures in polydimethylsiloxane–zeolite membranes, J. Membr. Sci. 415– 416 (2012) 635–643.
[36] S.J. Lue, S.F. Wang, L.D. Wang, W.W. Chen, K.M. Du, S.Y. Wu, Diffusion of multicomponent vapors in a poly(dimethyl siloxane) membrane, Desalination 233 (2008) 277–285.
[37] S.J. Lue, W.T. Wang, K.P.O. Mahesh, C.C. Yang, Enhanced performance of a direct methanol alkaline fuel cell (DMAFC) using a polyvinyl alcohol/fumed silica/KOH electrolyte, J. Power Sources 195 (2010) 7991–7999.
[38] S.J. Lue, H. Juang, S. Hou, Permeation of xylene isomers through supported liquid membranes containing cyclodextrins, Sep. Sci. Technol. 37 (2002) 463–480.
[39] Y.W. Rhee, S.Y. Ha, R.I. Masel, Crossover of formic acid through Nafion membranes, J. Power Sources 117 (2003) 35–38.
[40] C.C. Huang, Y.L. Liu, W.H. Pan, C.M. Chang, C.M. Shih, H.Y. Chu, C.H. Chien, C. H. Juan, S.J. Lue, Direct borohydride fuel cell performance using hydroxide-conducting polymeric nanocomposite electrolytes, J. Polym. Sci. Polym. Phys. 51 (2013) 1779–1789.
[41] J.F. Wu, C.F. Lo, L.Y. Li, H.Y. Li, C.M. Chang, K.S. Liao, C.C. Hu, Y.L. Liu, S.J. Lue, Thermally stable polybenzimidazole/carbon nano-tube composites for alkaline direct methanol fuel cell applications, J. Power Sources 246 (2014) 39–48.
[42] S.J. Lue, J.Y. Chen, J.M. Yang, Crystallinity and stability of poly(vinyl alcohol)-fumed silica mixed matrix membranes, J. Macromol. Sci. Part B – Phys. 47 (2008) 39–51.
[43] F.Y. Ban, S.R. Majid, N.M. Huang, H.N. Lim, Graphene oxide and its wlectrochemical performance, Int. J. Electrochem. Sci. 7 (2012) 4345–4351.
[44] K. Kunimatsu, T. Yoda, D.A. Tryk, H. Uchida, M. Watanabe, In situ ATR-FTIR study of oxygen reduction at the Pt/Nafion interface, Phys. Chem. Chem. Phys. 12 (2010) 621–629.
[45] K.T. Adjemian, S.J. Lee, S. Srinivasan, J. Benziger, A.B. Bocarsly, Silicon oxide

Nafion composite membranes for proton-exchange membrane fuel cell operation at 80–140°C, J. Electrochem. Soc. 149 (2002) A256–A261.
[46] X. Wang, L. Song, H. Yang, W. Xing, B.J. Kandola, Y. Hu, Simultaneous reduction and surface functionalization of graphene oxide with POSS for reducing fire hazards in epoxy composites, J. Mater. Chem. 22 (2012) 22037–22043.
[47] M.C. Hsiao, C.C.M. Ma, J.C. Chiang, K.K. Ho, T.Y. Chou, X. Xie, C.H. Tsai, L. H. Chang, C.K. Hsieh, Thermally conductive and electrically insulating epoxy nanocomposites with thermally reduced graphene oxide–silica hybrid nanosheets, Nanoscale 5 (2013) 5863–5871.
[48] A. Dimiev, D.V. Kosynkin, A. Sinitskii, A. Slesarev, Z. Sun, J.M. Tour, Layer-by-layer removal of graphene for device patterning, Science 331 (2011) 1168–1172.
[49] R. Kumar, C. Xu, K. Scott, Graphite oxide/Nafion composite membranes for polymer electrolyte fuel cells, RSC Adv. 2 (2012) 8777–8782.
[50] D.R. Dreyer, S. Park, C.W. Bielawski, R.S. Ruoff, The chemistry of graphene oxide, Chem. Soc. Rev. 39 (2010) 228–240.
[51] J.P. DeRocher, B.T. Gettelfinger, J. Wang, E.E. Nuxoll, E.L. Cussler, Barrier membranes with different sizes of aligned flakes, J. Membr. Sci. 254 (2005) 21–30.
[52] M.Z. Iqbal, M.S. Katsiotis, S.M. Alhassan, M.W. Liberatore, A.A. Abdala, Effect of solvent on the uncatalyzed synthesis of aminosilane-functionalized graphene, RSC Adv. 4 (2014) 6830–6839.